Fluorescence Microscopy of Nanochannel-Confined DNA

Chapter 9

Fluorescence Microscopy of Nanochannel-Confined DNA

Sriram KK, Fredrik Persson, Joachim Fritzsche, Jason P. Beech, Jonas O. Tegenfeldt, and Fredrik Westerlund

Abstract

Stretching of DNA in nanoscale confinement allows for several important studies. The genetic contents of the DNA can be visualized on the single DNA molecule level, and the polymer physics of confined DNA and also DNA/protein and other DNA/DNA-binding molecule interactions can be explored. This chapter describes the basic steps to fabricate the nanostructures, perform the experiments, and analyze the data.

Key words DNA, Nanochannels, Single molecule, Fluorescence

1 Introduction

Single DNA molecules stretch spontaneously in nanochannels due to the confinement. The stretching is entirely passive, and thus, no active application of force is required apart from the driving force to move the DNA into the nanochannel. In contrast to flow stretching or stretching using optical tweezers, no chemically attached anchor groups are needed. The first study of DNA in nanochannels was presented in 2004 [1], and since then, the field has been growing vastly with applications in several different fields of research [2].

There are a few important parameters to consider when dealing with confined DNA:

1. Contour length: total length of the DNA backbone, here denoted L.
2. Persistence length: length-scale over which the DNA can be considered a rigid rod, here denoted P.
3. Effective width: a measure of the width of the DNA, composed of the physical width of the DNA (~2 nm) and an electrostatic contribution. [3]. The effective width is here denoted w_{eff}.

Iddo Heller et al. (eds.), *Single Molecule Analysis: Methods and Protocols*, Methods in Molecular Biology, vol. 2694,
https://doi.org/10.1007/978-1-0716-3377-9_9,

When a long DNA molecule is free in aqueous solution, it forms a coil, often characterized by its radius of gyration (R_G). When confined in a tubelike channel with an average cross-sectional diameter D_{av} smaller than R_G, the DNA stretches out along the length of the channel. As long as the diameter of the channel is larger than P, the DNA can backfold and adopt an elongated coiled up conformation. In this regime, commonly denoted the deGennes regime, the DNA can be modeled as a series of noninteracting blobs, where the DNA inside each blob behaves as it would in free solution. This leads to an extension, r, of the DNA along the channel of [4]:

$$\frac{r}{L} \propto \left(\frac{w_{\text{eff}} P}{D_{\text{av}}^2} \right)^{1/3}$$

Fabricated nanochannels are more commonly rectangular in cross section. Here, D_{av}^2, the parameter relating to the diameter of the tube, can be replaced by the geometric average of the height, D_1, and the width, D_2, of the rectangular channel, $D_{\text{av}}^2 = D_1 D_2$ for $D_1 \sim D_2$ [5]. For situations where $D < P$, the DNA molecule cannot fold back on itself, and its extension can be described by a model developed by Odijk [6]. This is relevant for DNA not only in very small channels but also in studies of protein-DNA interactions where the resulting protein-DNA complex has an increased persistence length [7]. The extension, r, of the DNA along the channel is here ($B \sim 0.091$ [8]):

$$\frac{r}{L} \quad 1 - B \left[\left(\frac{D_1}{P} \right)^{2/3} + \left(\frac{D_2}{P} \right)^{2/3} \right]$$

From an experimental point of view, it is important to note that in both models r scales linearly with L. This means that a position along the stretched DNA can be directly related to a position along the contour of the DNA, that is, the sequence, with a resolution primarily determined by the degree of stretching and the optics of the microscope. While the simple expressions above give adequate accuracy for designing a nanochannel device, recent improved understanding makes it possible to predict the behavior of the confined DNA with much better accuracy [9, 10]. Note however that not only the geometry of the confinement but also the buffer conditions have a strong influence on the behavior of the DNA. For further insight regarding the polymer physics of confined DNA, the authors recommend references [2, 11–13]. There is also a vast literature on general polymer theory, notably the books by deGennes [14], Doi and Edwards [15], and Rubinstein and Colby [16].

The first experimental studies of DNA in nanochannels were devoted to studies of DNA conformation and dynamics [1, 12, 17, 18]. Since these first experiments, the field has expanded in three

main directions [2]. Studies of the polymer physics of DNA have provided novel, more accurate theories about how DNA behaves in confinement [10, 19–21]. Even nearly two decades after the first experimental studies, there is still interest in understanding the physics of DNA confined in nanofluidic channels [22–24].

DNA-protein interactions have continued to receive significant attention with a main focus on proteins that change the physical properties of DNA. The first studies involving DNA-protein interactions showed the possibility of using a nanofluidic device to observe DNA restriction using enzymes like Sma1 and Sac1 [25] as well as lac-repressor binding to specific locations on single DNA molecules [26]. Although many studies were done subsequently toward utilizing nanofluidics to study DNA-protein interactions, the focus has been on using nanofluidics as a platform to visualize the end product formed from the interaction between DNA and the protein of interest. Examples include phosphorylated CtIP, a cofactor of the MRE11-RAD50-NBS1 (MRN) complex shown to promote annealing of broken DNA ends [27], alpha-synuclein that increases the stiffness of DNA [28], Hfq mediated compaction of DNA [29], and HIV-1 nucleocapsid chaperone protein that compacts DNA [30]. However, recent developments in nanochannel device fabrication enable real-time studies of DNA-protein interactions [31–33]. This has opened up the possibility of actively exchanging proteins/reagents, while the DNA molecule is still in the nanochannel environment, facilitating dynamic interactions to be studied in situ.

Optical DNA mapping is the third main direction of studies of DNA in nanochannels that has developed vastly during the last years. Optical DNA mapping has been commercialized by BioNanoGenomics [34], and the goal of this technique is to visualize the structure of the genetic sequence of large (several hundred kilobasepairs) single DNA molecules. To do this, the DNA has to be sequence-specifically labeled, and this is done in two main different ways. One way is to use enzymes to attach fluorophores at specific sequences [35, 36], while the second relies solely on non-covalent interactions between DNA and fluorophores as described below [37, 38]. Finally, in analogy to standard gel electrophoresis, the nanochannels can be used to merely measure the length of DNA fragments. This may be used to size plasmids [39] and in combination with restriction enzymes for restriction mapping [25]. Recently, there has also been an attempt at mapping single-stranded DNA (ssDNA) using nanochannels [40]. ssDNA has a persistence length (P) of only a few nanometers and has the tendency to form self-annealed structures, but the use of a diblock polypeptide copolymer has circumvented this issue.

2 Materials

2.1 Fabrication of Chips

There are a multitude of ways to fabricate nanostructured chips depending on the facilities and equipment available (*see* **Note 1**) [41]. We present two fabrication schemes here, one based on fused silica and one based on silicon.

For fabrication in fused silica, the following is needed:

1. Fused silica wafers (Available from Hoya Corporation).
2. 110 μm thick fused silica coverslips for sealing of the chips. The thickness is optimized for compatibility with oil immersion objectives (Available from Valley Design).
3. Access to cleanroom equipment for photo (UV) and electron-beam (e-beam) lithography and reactive ion etching (RIE) as well as standard resists (e.g., Shipley or AZ (photo lithography) and ARP or ZEP (e-beam lithography)) and chemicals from any large supplier.

For fabrication in silicon, the following is needed:

1. Silicon wafers (Available from SiMat).
2. 170 μm thick borosilicate coverslips for sealing of the chips. The thickness is optimized for compatibility with oil immersion objectives (Available from SiMat).
3. Access to cleanroom equipment for photo (UV) and electron-beam (e-beam) lithography and reactive ion etching (RIE) as well as standard resists (e.g., Shipley or AZ (photo lithography) and ARP or ZEP (e-beam lithography)) and chemicals from any large supplier.

2.2 Chemicals

Two important additives are β-mercaptoethanol (BME) (*see* **Note 2**) for suppression of photobleaching and polyvinylpyrrolidone (PVP) (*see* **Note 3**) for suppression of electroosmosis when using electrophoresis. Note that genomic length DNA should be handled with wide-orifice pipettes to avoid shear-induced breakage (provided by, e.g., molecular bioproducts).

2.3 Buffers

2.3.1 Buffer for DNA Experiments

Tris-Borate-EDTA (TBE) is a standard buffer for DNA studies, especially for electrophoresis, due to its low conductivity that ensures a low degree of Joule heating (as the borate is a suspected CMR (carcinogenic, mutagenic or toxic for reproduction), TAE is an alternative that is often used, *see* **Note 4**). TBE buffer consists of:

1. *Tris (tris(hydroxymethyl)aminomethane):* Buffering agent for slightly basic conditions (pH = 7.9).
2. *Boric acid:* Weak acid that improves the buffering capabilities of Tris.

3. *EDTA (Ethylenediaminetetraacetic acid):* Chelating agent that scavenges multivalent metal ions, in particular magnesium (Mg^{2+}). Since multivalent metal ions are common co-factors for many enzymes, like nucleases that digest DNA, the removal of these ions will prevent enzymatic degradation of DNA.

2.3.2 Protocol for Preparing 1 L 5× TBE Buffer

1. Prepare 0.5 L of 0.5 M EDTA solution by weighing out 93.06 g of disodium EDTA (372.24 g/mol) and adding it to 350 mL of water (*see* **Note 5**). EDTA will not go into solution until pH is adjusted to 8.0. Add NaOH pellets to the solution, one by one, while stirring vigorously on a magnetic stir plate. Monitor solution pH using a digital pH meter so as not to overshoot. Bring the final solution volume to 0.5 L with water.
2. Prepare a 5× TBE solution by adding 20 mL of 0.5 M EDTA solution from **step 1**, 54 g of Tris (121.1 g/mol) and 27.5 g of boric acid (61.8 g/mol) to 800 mL of water. Then adjust pH to 8.0–8.5 by adding HCl while monitoring pH. Bring final solution volume to 1 L with water.
3. Autoclave buffer.

   The stock buffer can be diluted to any arbitrary ionic strength. For the following steps, 0.5× TBE buffer is used as an example. Note that the stretching of confined DNA varies significantly with ionic strength [42], and for particular applications, such as DNA mapping, the DNA should be stretched out as much as possible and hence a low ionic strength is used.
4. Dilute the 5× TBE buffer ten times. Then use a syringe with a 0.2 μm filter to aliquot approximately 1.2 mL of buffer into a large number of 1.5 mL microcentrifuge tubes. Store these tubes in the refrigerator for future use. Degas the tubes for at least 2 h prior use. The final 0.5× TBE solution contains 44.6 mM Tris, 44.5 mM boric acid, and 1 mM EDTA and has an ionic strength of approximately 15 mM at pH 8.5.

2.3.3 Protocol for Staining 1 mL of 10 μg/mL DNA at a dye:bp Ratio of 1:10 in 0.5× TBE Buffer

Always use wide-orifice pipette tips to handle DNA solutions.

1. Create 250 μL of 50 μg/mL solution of DNA in 0.5× TBE (*see* **Note 6**).
2. Pipette 769 μL of 0.5× TBE buffer into a separate 1.5 mL microcentrifuge tube.
3. Pipette 47.5 μL of 0.5× TBE buffer into a 0.65 mL tube. Add 2.5 μL of YOYO-1 from the stock solution (1 mM). This creates a 50 μM dye solution. Work in low light from now on to avoid bleaching of the dye.
4. Pipette 31 μL of the 50 μM dye solution from **step 3** into the buffer-filled tube from **step 2**. This creates a solution with a dye concentration of 1.55 μM. Vortex and centrifuge the solution to evenly distribute the dye.

5. Pipette 200 μL of DNA from **step 1** into the buffer filled tube from **step 4**. Do *NOT* ever vortex or centrifuge solutions containing DNA – that will fragment the DNA. In order to mix the DNA, use a wide-orifice tip and gently pipette a part of the solution a minimum of three times while evenly distributing the ejected solution throughout the tube.
6. To evenly distribute the dye throughout the population of DNA molecules, wrap the tube in aluminum foil and heat the solution to 50°C for 3 h and then store at 4°C. An alternative for efficient equilibration is to prepare the samples at high ionic strength (5× TBE), where equilibration is fast, and subsequently dilute the sample to the desired ionic strength [43].

To obtain an optical map of the DNA or to study DNA-protein interactions, more intricate sample preparations are needed, *see* **Notes 7** and **8**.

2.3.4 Protocol for Preparing 400 μL Loading Buffer and 100 μL DNA in Loading Buffer

1. Mix 485 μL of degassed buffer with 15 μL of BME (*see* **Note 9**) in a 0.65 mL microcentrifuge tube. BME will collect at the bottom of the tube, so mixing by pipetting and/or vortexing is essential at this stage. Note that vortexing should *not* be performed after the DNA has been added. Below we will refer to this as the *loading buffer*.
2. Pipette 95 μL of the loading buffer into a 0.65 mL microcentrifuge tube.
3. Add 5 μL of the 10 μg/mL solution of stained DNA using wide-orifice pipettes. Mix the solution very gently with the pipette. Work in low light to protect the DNA and wrap the tube in aluminum foil once the DNA-solution is made. Alternately, use a light safe microcentrifuge tube (LightSafe available from Sigma-Aldrich or LiteSafe from ArgosTechnologies). Below we will refer to this as the *DNA loading sample*.

2.4 DNA Samples

In order to characterize the experimental techniques, it is necessary to use monodisperse DNA. There are a few different purified monodisperse DNA solutions commercially available, and using restriction enzymes, different size distributions can be obtained. Table 1 lists a few common examples of commercially available, purified and monodisperse DNA.

2.5 Fluorescence Microscopy

For a thorough introduction to microscopy, the authors recommend the MicroscopyU website from Nikon (www.microscopyu.com), especially the tutorial section on fluorescence microscopy (www.microscopyu.com/articles/fluorescence/index.html), as well as Ref. [44].

Table 1
Selection of commercially available DNA molecules

Name	Length [kbp]	Supplier
λ-DNA	48.5	New England Biolabs
λ-DNA concatamers (in gel)	$48.5 \times n$ ($n = 1...\sim20$)	New England Biolabs
T4GT7-DNA	166	Nippon gene
Charomid 9 (circular)	19.7–42.2	Nippon gene
T7	39.9	Boca scientific, Bioron GmbH

Due to the low light levels and the risk of photodamaging the DNA, the optical system must be designed to maximize photon detection probability and signal-to-noise ratio. Key considerations are:

1. High-quality filters with high transmission (~90%) in the wavelength region relevant for the dye used and low transmission in the rest of the spectrum, corresponding to a high optical density (OD > 5).
2. Objectives (40–100×) with high numerical apertures (NA). Oil immersion objectives readily achieve NA of 1.4 and are perfectly suited for devices sealed with standard coverslips with a thickness of 170 μm. To combine a good NA and a large WD, a 60× water immersion objective with an NA of 1.0 and a WD of 2 mm, originally designed for electrophysiology by Nikon, can be used. This provides sufficient clearance in situations when normal cover glass cannot be used.
3. A detector with high quantum efficiency (QE) and low noise. Electron-multiplying CCDs (EMCCD) have an integrated noise-less amplification on the CCD chip. As opposed to intensification technologies based on multichannel plates, the EMCCD is not easily damaged by excessive light levels. The EMCCD can be back-thinned to allow for a QE approaching 90–95% over the visible spectrum. Less expensive EMCCDs are not back-thinned and thus suffer from QE that are roughly a factor of two lower. To minimize thermal noise, the EMCCD is normally cooled from −50°C to −100°C in modern cameras. EMCCD cameras are available from, for example, Andor, Photometrics, and Hamamatsu. In recent years, sCMOS cameras with QE of ~95% have become available, providing larger field-of-view and high-resolution images. For example, Photometrics prime 95B is an example of such an sCMOS camera.
4. Image acquisition requires dedicated software. Commercial fluorescence microscopes and cameras often come with

proprietary software. An alternative is to use μManager, an open-source software for control and automation of microscope hardware (https://micro-manager.org/).

See **Notes 10** and **11** for examples of additional optical tools and technologies.

2.6 Addressing the Chip

The two most common ways of manipulating DNA in fluidic systems are by electrophoresis or pressure-driven fluid flow. In order to have both these capabilities, a chip holder with both electrical and gas pressure connections to internal reservoirs can be used [37]. The holder can be fabricated in Lucite® (PMMA), allowing the sample to be illuminated from the top and making it easy to detect bubbles trapped in the reservoirs in the chip holder. However, Lucite® has poor resistance to solvents, as it swells and dissolves easily. For experiments involving more aggressive solvents, a holder made in PEEK (PolyEtherEtherKetone) is more suitable, but then the holder is opaque.

An updated holder design is shown in Fig. 1. It has a modular design where the chip is glued to a plastic frame that is readily mounted in the stage adapter. This way the integrity of the chip is better protected as compared to previous designs.

Pumps are needed for controlling DNA using pressure-driven flow. Standard diaphragm pumps capable of producing pressures of up to 5 Bar are sufficient in most cases (available from VWR). When using pressure-driven flow, the pressure is routed through a network of valves giving the possibility of applying pressures to selected reservoirs while others are kept at ambient pressure. To control the pressure, a needle valve can be used as a leak valve, which enables the pressure to be controlled with an accuracy of down to ±2 mBar. Accessories such as manifolds, needle valves, and tubing to direct and control the pressure are available from Cole

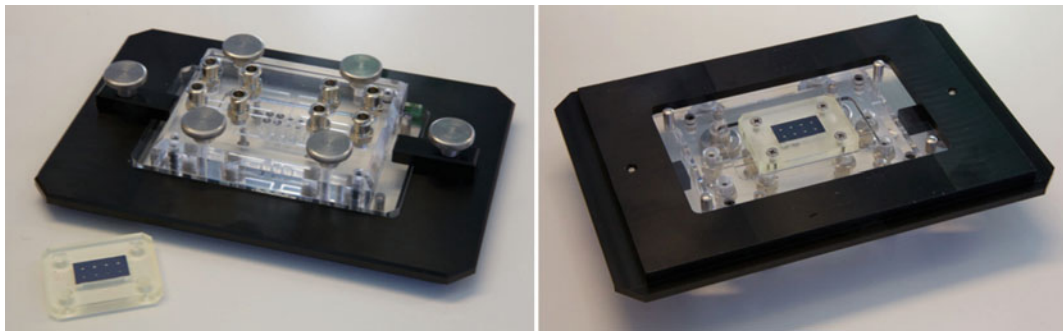

Fig. 1 Example of chuck for mounting samples. Modular design with separate parts for frame and fluidics. The device chips are mounted in plastic holders for easy handling. Eight reservoirs linked by o-rings to the fluidic access holes on the chip. Reservoirs are individually addressable by pressure and electrical connections. (Left) Top view. Device chip is not mounted. (Right) Bottom view with mounted device chip

Parmer. Note that by using nitrogen as a driving gas, the oxygen in the sample buffer is depleted, and photobleaching and photodamage are minimized.

When using electrophoresis to control the DNA, a power supply and electrodes are needed. Platinum wires dipped into the DNA solution in the reservoir are often sufficient as electrodes. The electrophoretic mobility of DNA is on the order of 1 μm/s per V/cm.

2.7 Data Analysis

Commonly used software packages for data analysis are as follows:

1. ImageJ: A Java™-based freeware image processing and analysis software developed at the National Institutes of Health, USA (http://rsbweb.nih.gov/ij/). The software benefits from the extensive use of open-source plug-ins developed by users. The MBF plug-in set from the Biophotonics Facility at McMaster University is recommended (http://www.macbiophotonics.ca/imagej/).
2. MATLAB: A common high-level technical computing language from The Mathworks™.
3. FreeMat: Open-source freeware available at http://freemat.sourceforge.net/
4. GNU Octave: Freeware available at http://www.gnu.org/software/octave/

Data analysis in optical DNA mapping is more intricate than simply determining the sizes of DNA molecules *see* **Note 12**.

3 Methods

3.1 Design and Fabrication of Chips

3.1.1 Design

A careful design of the DNA-visualization device is crucial for its user-friendliness. Typically, two or four U-shaped inlet channels (50 μm × 1 μm, each connected to two reservoirs) for efficient fluid transport are combined with nanoscale channels for stretching of the DNA. In this way, the sample can be transported quickly through the large channels to the entrance of the nanochannels by applying a driving force across the microchannel, enabling rapid exchange of buffer. Using nanochannels of dimensions 100 nm × 100 nm ensures a relatively high degree of DNA stretching (~60%) without encountering many of the problems that appear when the channel size approaches the persistence length of DNA (~50 nm). The degree of stretching can be tuned by altering the buffer conditions [42], such as the ionic strength.

See **Notes 13–15** for examples on how to include extra functionalities on the chip.

3.1.2 Fabrication

When fabricating nanofluidic channels for optical observation of stretched DNA, there are some requirements to consider:

1. The channels should be sealed.
2. At least one side (substrate or lid) must be optically transparent.
3. The surface of the channels should be negatively charged with a minimal roughness to prevent sticking and entanglement of the DNA.
4. The material used should be hydrophilic to allow for easy wetting of the channels.

In the following section, two commonly used fabrication processes based on fused silica and on composites of silicon and borosilicate glass are outlined. Note that to be compatible with electrophoresis, the devices should be made in glass or silica, or, if silicon is used, that the surface oxide is of high enough quality such that no pinholes are formed.

A full-scale cleanroom, with spinners for resist deposition, mask aligners for exposure of micron scale patterns and an electron-beam writer for definition of nanoscale structures, is required for both fabrication schemes (*see* **Note 16**). Reactive-ion etchers are used for etching channels with straight walls.

In order to align the nanostructures and the microchannels, it is useful to first define alignment marks in the wafer periphery. This can be done by either etching or depositing metals on the wafer (*see* **Note 17**), the latter described below. It is assumed that the cleanroom used has its own standard processes for the following steps.

3.1.3 Definition of Alignment Marks

Fused silica:

1. Treat the fused silica wafers with *hexamethyldisilazane (*HMDS) to increase resist adhesion.
2. Spincoat and bake a combination of resists used for liftoff, for example, a LOR/AZ or other similar sandwich constructs, to enable a pattern with an undercut.
3. Expose and develop the resist to create the undercut structure.
4. Run a low-power oxygen descum plasma to remove remaining resist residues.
5. Evaporate a 5 nm Cr (or Ti) adhesion layer and subsequently a 50–80 nm thick Au layer.
6. Strip the resist using a chemical stripper, for example, Microposit Remover 1165 or acetone (*see* **Note 18**).

Silicon–borosilicate glass:

1. Thermally oxidize the surfaces of the Si-wafers to a thickness greater than the intended depth of the microchannels in order to accommodate both nanochannels and microchannels in the oxide layer. The oxide layer is typically in the range of 1–2 μm.

2. See the processing **steps 1–6** above for the case of fused silica.
3. Alternately, one can make the alignment marks using a positive photoresist (e.g., S1813) in **step 2**, develop the photoresist to form the structure **(step 3)** and etch them into fused silica or silicon-borosilicate glass using RIE. In this case, the metal deposition step described in **step 5** is not needed.

3.1.4 Definition of Nanochannels

Fused silica:

1. Treat the fused silica wafers with HMDS to increase resist adhesion.
2. Spincoat and bake a 150–250 nm thick layer of ZEP520A e-beam resist. ZEP is chosen because of its good dry-etch resistance. AR-P 6200 is a suitable alternative for ZEP520A. Other resists can be used but they often require deposition of an extra metallic etch mask.
3. Thermally evaporate 20 nm Cr on top as a discharge layer. (This is only needed when working with insulating substrates such as fused silica.)
4. Expose the resist (exposure dose approximately 280 $\mu C/cm^2$ at 100 kV).
5. Remove the Cr layer using Cr wet etching.
6. Develop the resist using, for example, n-Amylacetate followed by rinsing with isopropanol.
7. Run a low-power oxygen descum plasma in order to remove remaining resist residues.
8. Etch the nanochannels into the fused silica using RIE with CHF_3/CF_4 chemistry.
9. Strip the resist using a chemical stripper, for example, Microposit Remover 1165.

Silicon–borosilicate glass: See the processing **steps 1–2, 4, 6–9** above for the case of fused silica. Note that application and removal of a discharge layer (**steps 3** and **5**, respectively) are not needed when processing conductive substrates.

3.1.5 Definition of Microchannels (Fused Silica and Silicon–Borosilicate Glass)

1. Treat the wafers with HMDS to increase resist adhesion.
2. Spincoat and bake a 2–5 μm thick layer of photoresist, for example, an AZ resist, that has relatively high etch resistance.
3. Expose and develop the resist.
4. Run a low-power oxygen descum plasma in order to remove remaining resist residues.
5. Etch the microchannels (approximately 1 μm deep) using RIE with CHF_3/CF_4 chemistry.
6. Strip the resist using a chemical stripper, for example Microposit Remover 1165 or acetone.

3.1.6 Processing of Access Holes

Fused silica: There are a multitude of ways to produce access holes through a wafer (*see* **Note 19**). Here, we describe a setup based on powder blasting.

1. Spincoat at least 5 μm photoresist on both sides of the wafer.
2. Cover the backside (i.e., the nonstructured side) with an adhesive plastic film, for example, 70 μm thick Nitto SWT 20 film (*see* **Note 20**).
3. Make holes through the film over the reservoir structures using a scalpel or, for example, laser ablation.
4. Powder blast using 50–110 μm sized Al_2O_3 particles from the backside of the wafer (i.e., the nonstructured side). A small powder-blasting tool and powder can be obtained from Danville Eng.
5. Remove the film, strip the resist in a chemical stripper and/or acetone and carefully clean the wafers in an ultrasonic bath.

Silicon–borosilicate glass:

1. Deposit 150 nm Al on the processing side of the silicon wafer by either sputtering or evaporation.
2. Spincoat and bake a 2–5 μm thick layer of photoresist, for example an AZ resist.
3. Expose and develop the resist.
4. Run a low-power oxygen descum plasma in order to remove remaining resist residues.
5. Remove the Al-layer in the openings of the resist with Al-wet etch that is compatible with the resist being used, for example, 80% H_3PO_4 + 5% HNO_3 + 5%HAc + 10%H_2O.
6. Etch through the Si-wafer with a deep reactive-ion etch (Bosch) process. Note that this processing step will typically consume the applied photoresist and thus relies on the Al-layer as a hard mask.
7. Remove the Al-mask with Al-wet etching.

3.1.7 Sealing of the Chips

The last step in the production of the chips is sealing. This can be done in several different ways depending on the material of the chips (*see* **Note 21**). Fused silica can be bonded covalently via condensation of hydroxyl groups when two surfaces are brought together. Table 2 summarizes two standard ways of creating a high density of the necessary hydroxyl groups, involving thorough cleaning to remove organic residues and subsequent surface activation (*see* **Note 22**).

For the RCA-based method, the hydrogen peroxide should be added after the mixture has reached the correct temperature to avoid disintegration of the hydrogen peroxide.

Table 2
Two fusion-bonding protocols for fused silica (*see* Note 22)

RCA-based		Piranha-based	
Chemical	**Time**	**Chemical**	**Time**
RCA2 at 80°C (1:1:5 HCl:H_2O_2:H_2O)	10 min	Piranha (1:3 H_2O_2:H_2SO_4)	20 min
Rinse carefully with DI water for 5 min			
RCA1 at 80 °C (1:1:5 NH_2OH:H_2O_2:H_2O)	10 min	Ammonium hydroxide (NH_4OH)	40 min
Rinse carefully with DI water for 5 min			
Blow dry in N_2			
Press together by hand to form a prebond			
Anneal at 1050°C for at least 3 h (ramp temperature at approximately 300°C /h for both heating and cooling.)			

3.2 Chemicals

When studying single DNA molecules, it is very important that the molecules are kept in a controlled environment and not subjected to reactive contaminants such as radicals or enzymes that damage or digest DNA. Some of these enzymes, such as endonucleases, are present on our skin in order to break down foreign DNA that we come in contact with. It is therefore crucial that gloves are worn at all times when handling DNA and that all tools and pipette tips that come in contact with either the buffer or the DNA samples have been autoclaved or sterilized in another way, for example, by wiping them with ethanol.

3.2.1 Fluorescent Labeling of DNA

Dimeric cyanine dyes like YOYO®-1 (YOYO) (Invitrogen, Carlsbad, California, USA) are extensively used for imaging single DNA molecules due to their high binding affinity to DNA ($K_A = 10^{10}$–10^{12} M^{-1}) and a fluorescence enhancement upon binding to DNA of over 1000, which ensures a low fluorescence background from unbound dye molecules [45]. Figure 2 shows the absorption and emission spectra as well as the chemical structure of YOYO [46]. Staining of the DNA with intercalators affects the physical properties of the DNA. The effect on the persistence length of the DNA due to intercalation has been an area of controversy with a wide range of reported effects. Recently, it has been concluded that the persistence length is unaffected [47]. The contour length of DNA is however increased by approximately 0.68 nm per intercalating YOYO molecule (one basepair (0.34 nm) per intercalation event) [48, 49] at moderate binding densities.

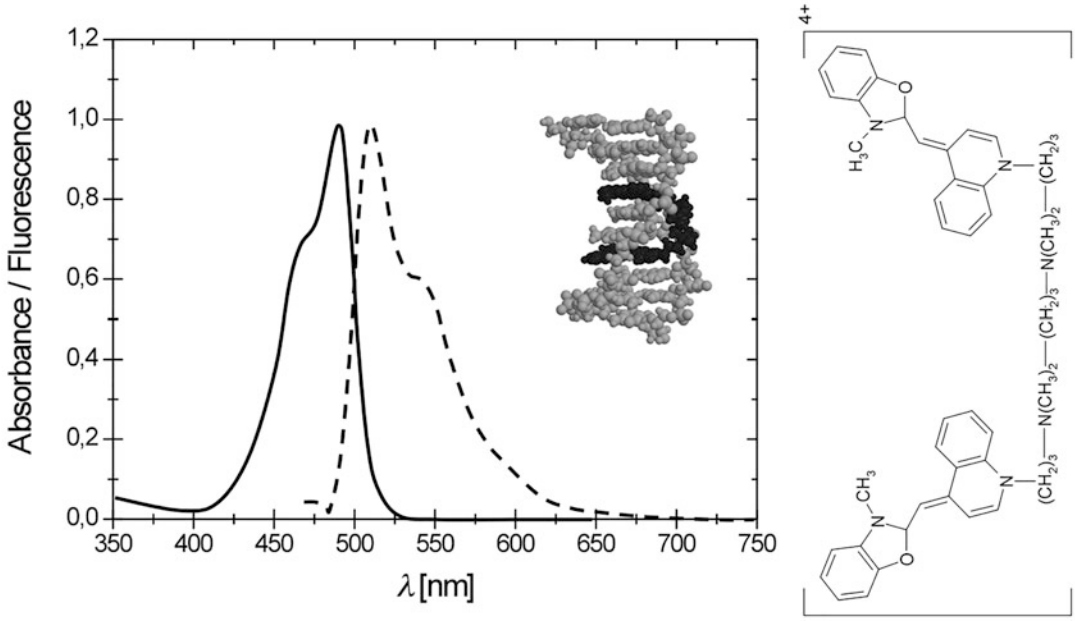

Fig. 2 (Left) Excitation (solid) and emission (dashed) spectra of YOYO®-1. (Adapted from data from Invitrogen). Inset: TOTO®-1 intercalating in DNA, visualized using the open-source viewer JMol. The structure (PDB ID: 108D) was determined by nuclear magnetic resonance [46]. (Right) Chemical structure of YOYO®-1

When staining the DNA, it is important to know the resulting dye:bp ratio ([dye molecule]:[basepair]). The easiest way of calculating this is to use the molar concentration of the dye and DNA, respectively. If the concentration of DNA is known in μg/mL, it is easily converted using the molar mass of one DNA basepair (bp), $M_{bp} = 618$ g/mol. The DNA concentration can also be determined by absorbance measurements, using the molar absorption coefficient for DNA at $\lambda = 260$ nm, $\varepsilon_{260} = 13{,}200\ \mathrm{cm}^{-1}\ \mathrm{M}^{-1}$ (basepair) or 50 μg/mL for OD 1 (1 cm optical path length). Knowing the molar concentrations of the DNA and the dye, the dye:bp ratio is readily obtained. In the case of dimeric cyanine dyes, like YOYO, the dye concentration should not exceed a value corresponding to a dye:bp ratio of 1:5 in order to avoid crowding of dye on the DNA. It is important to note that the binding constant of YOYO decreases significantly at high ionic strength. This means that at higher ionic strengths, the amount of dye bound will not correspond to the amount of dye added [43].

3.3 Running Experiments (Loading of DNA)

Prior to mixing the loading buffer, the TBE buffer can be degassed in a vacuum chamber for 2 h in order to reduce the amount of dissolved air in the system and to avoid bubble formation in the channels. The degassing process can be shortened to about 10–20 min by ultrasonic agitation. If nitrogen is used to pressurize the system instead of air, the degassing can be shortened or even

completely skipped. Fresh loading buffer should be prepared in conjunction with every experiment, since the BME degrades with time (*see* **Note 23**).

Use the loading buffer to wet the chip, either before mounting in the chuck or after. Placing droplets over the fluidic access holes is normally sufficient to wet the chip by capillary forces (*see* **Note 24**). Remaining air bubbles can be removed by applying a pressure across the channels. Using degassed buffer solution during experiments ensures that bubbles formed during the capillary wetting [50] are absorbed into the liquid and also prevents the DNA from degrading.

When the chip is properly wetted, the DNA loading sample is added to the desired reservoirs and loading buffer to the remaining reservoirs. For experiments regarding DNA-protein interactions, it is important to passivate the nanochannels before running the experiments to avoid nonspecific binding of the proteins to the channel walls, *see* **Note 25**.

The DNA can be moved through the chip by electrokinetic transport or pressure-driven flow. A pressure difference of approximately 100 mBar results in reasonable sample velocities when transporting the DNA in the micron-sized channels, from the inlet reservoirs to the nanostructures. Once the DNA molecules are in close proximity to the inlets of the nanochannels, the driving force is shifted so that it is applied across the nanochannel array instead. At this point, a low driving pressure makes it possible to collect a desired amount of DNA at the entrance of the nanochannels due to the entropic barrier. The most convenient way to subsequently introduce DNA into the nanochannels is to pulse the pressure, switching rapidly between a low pressure and 1–3 Bar. When the DNA molecules of interest are in the nanochannels and in the field of view of the CCD, stacks of images of at least 200 frames are recorded (*see* **Note 26**). During the measurements, the coordinates of at least two alignment marks on the chip as well as the stage coordinates for all the recorded stacks can be recorded. This allows for both rotational correction as well as accurate localization of the molecule within the fluidic network in the case of a more intricate design of the chip.

There are a few things to be aware of during image/data acquisition:

1. If one of the ends of the DNA molecule appears much brighter, it might have been folded while entering the nanochannel. Given time (usually minutes) the end will unfold [51], else the molecule can be pushed out into the microchannels and re-injected into the nanochannels.
2. A small pressure offset when using pressure-driven flow can cause the molecule to not be in its equilibrium state while imaging.

3. Photonicking may cause the DNA to be cut into smaller pieces while imaging. However, the ordering of the fragments will not change since two pieces cannot diffuse past each other while confined in a nanochannel (although very short fragments can pass).
4. During long imaging periods, the molecules will most likely fade significantly in fluorescence intensity due to photobleaching, especially in the absence of BME.
5. The DNA present close to the nanochannels can suffer from some degree of photobleaching and photonicking during imaging of the DNA in nanochannels. Therefore, an important consideration is to make sure that the illuminated area does not extend beyond the region of interest, if necessary using the field aperture.
6. DNA molecules may become pinned at one or several points along their length due to interactions with the surface of the channel. Pinned molecules are easy to identify and exclude from analysis.

The techniques used to fabricate nanochannel chips are time-consuming and expensive. It is therefore of interest to clean and reuse devices if possible. This can be done without removing the chip from the holder. The basic idea is to thoroughly remove all the running buffer and the sample from the entire chip and chip holder, replacing it with DI water. DI water should be flowed through the device at maximum pressure in various directions, while repeatedly replacing the solution in the reservoirs with clean DI water, until no sample can be seen. Illuminating the important areas of the chip with maximum power can help to break up/photo-bleach any stuck DNA or background fluorescence due to stuck dye. Alternately, the chip can be flushed with a detergent like sodium dodecyl sulfate (SDS, available from Sigma-Aldrich), followed by thorough rinsing with DI water. Close attention to cleaning can make it possible to use chips for many experiments over several months.

3.4 Data Analysis

To extract essential parameters from the movies (or rather stacks of images) of DNA molecules confined in a nanofluidic structure, a simple pattern recognition and fitting script can be used [1] The key steps of the analysis are listed and explained below.

1. The position of the DNA molecule is detected. A region of interest (ROI) is created around the molecule and the rest of the image is discarded in order to reduce the amount of data to store (Fig. 3a) [52].
2. The pixels are summed over the width of the extended DNA yielding a one-dimensional intensity profile of the molecule.

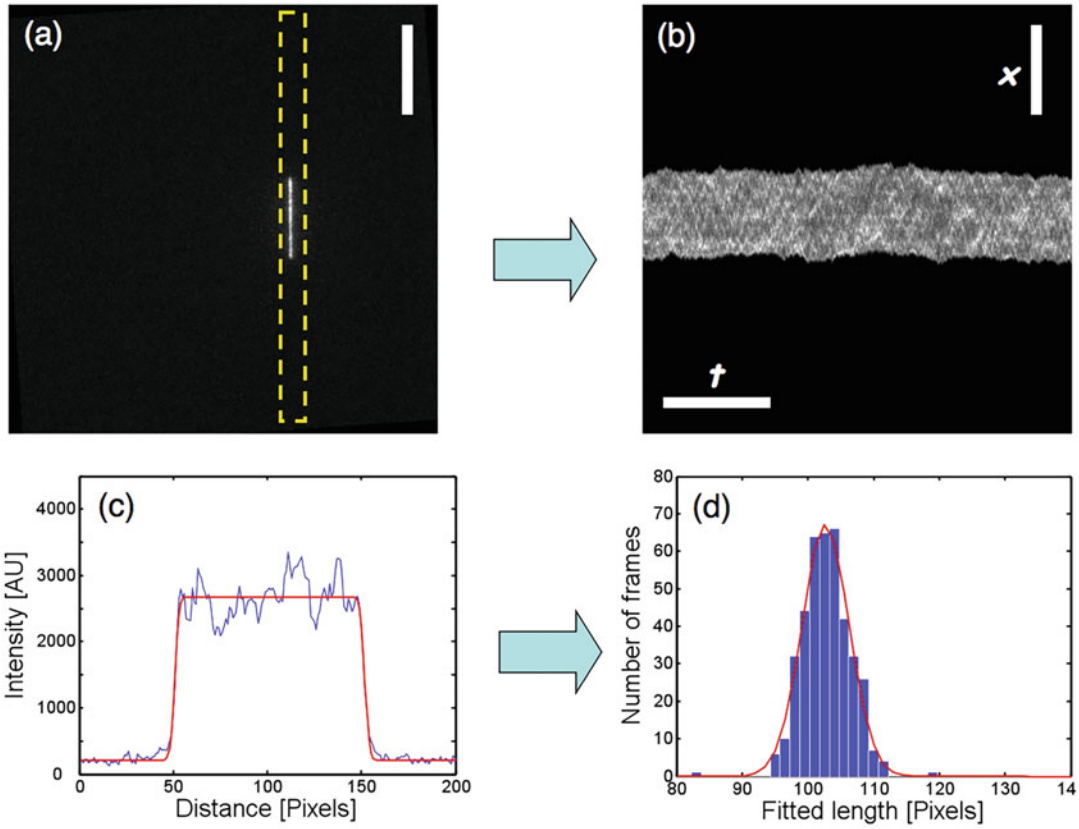

Fig. 3 (**a**) The first fluorescence image in an image stack. A box is drawn enclosing the extended DNA molecule. The scale bar corresponds to 20 μm. (**b**) Time trace, also referred to as kymograph, obtained by averaging over the molecule shown in (**a**) in the direction transverse to the DNA extension for every frame. Each column of pixels corresponds to the averaged intensity profile of one frame. The scale bars correspond to 20 μm and 10 s, respectively. (**c**) The intensity profile *I*(*x*) and the corresponding fit for one column of the time trace. (**d**) A histogram over all the fitted lengths from one movie containing 400 frames. The data is well described by a Gaussian distribution (solid line). (Reproduced with permission from reference [52])

3. **Step 2** is repeated for each frame in the movie, except that the molecule is identified based on its position in the previous frame. Stacking these intensity profiles next to each other yields a timetrace (also known as a kymograph) (Fig. 3b). In this way, a whole movie can be reduced to one single composite image.
4. The intensity profiles are fitted to a model profile, described below, by a least-square algorithm (Fig. 3c). This fitting provides the center position, intensity (with subtracted background) and length of the DNA for each frame in the original movie

The model intensity profile, $I(x)$, consists of a convolution of a modified box function (height I_0, length L_X) with a Gaussian point-spread function (PSF), with a full width at half maximum (FWHM)

of $2.35\sigma_0 = 0.61\lambda/\mathrm{NA}$ (λ is the wavelength of the light and NA is the numerical aperture of the objective) [1]. The model is represented by:

$$I(x) = I_{\mathrm{bg}} + \frac{I_0}{2} \times \left[(1-B)\mathrm{Erf}\left(\frac{x-x_0}{\sigma_0\sqrt{2}}\right) - (1+B)\mathrm{Erf}\left(\frac{x-(x_0+L_0)}{\sigma_0\sqrt{2}}\right) \right],$$

where I_{bg} is the background intensity value, B is a numerical factor introduced to allow for a nonconstant background, Erf is the error function, and x_0 is the center position of the box function (*see* **Note 27**).

It is important to realize that the biologically relevant gauge of resolution in these experiments is basepairs and not nanometers or pixels. Standard fluorescence microscopy has a resolution limited by diffraction to roughly half the wavelength of the detected light. The resolution in basepairs is determined by the degree of DNA stretching, the DNA fluctuations, and the total photon budget. Thus, maximum resolution is obtained in channels with the smallest possible cross section yielding fully stretched DNA with a minimum of thermal fluctuations. In practice, there is an optimum resolution for each experiment. Therefore, it is important to design the experiments accordingly. For example, studies of a selected region of interest along the genome may require the highest possible resolving power, requiring extensive efforts in terms of data acquisition, storage and handling. In some applications, the resolving power per se is not relevant; instead, the positioning of one or more specific labels contains the important information. In this case, the measurement uncertainty scales roughly as $1/\sqrt{N}$ where N is the number of detected photons, giving accuracies approaching a single nanometer [53].

The exact degree of stretching for a particular experimental condition can be determined using a DNA of known length, such as λ-DNA (from NEB), as reference.

For experiments regarding optical DNA mapping, the data analysis is more intricate, *see* **Note 12** for an example regarding competitive binding-based optical DNA mapping.

4 Notes

1. One common fabrication method uses nanoimprint lithography (NIL). This has the benefit that it is possible to order finished master stamps commercially (available from NIL Technology, Denmark), thus eliminating the need for an electron-beam lithography system. A common mass production technique, capable of defining nanostructures, is injection molding.

With suitable choice of low-fluorescence polymer matrix, it may prove useful for large series of devices. Although focused ion beam (FIB) milling is a slow linear technique, it may find use for creating complicated three-dimensional structures with resolution comparable to that of electron-beam lithography. Direct laser writing systems (available from Nanoscribe GmbH, Germany) are now also capable of creating complex three-dimensional structures with feature sizes below 100 nm.

A multitude of more exotic alternative fabrication techniques are described in the literature.

2. 0.1 M dithiothreitol (DTT) can replace BME as reducing agent.
3. POP6 (Performance Optimized Polymer 6) from Applied Biosystems can be used as an alternative to PVP.
4. TAE buffer is a useful alternative to TBE that replaces the borate with acetate. While borate has been identified as a substance that may pose risks with respect to CMR, acetate is considered a safe alternative. Compared to TBE, it has less buffering capacity, and for running gels, it must be exchanged more often. Standard concentration is 1× TAE: 40 mM TRIS acetate and 1 mM EDTA. TAE is readily available in 50× solution, or it can be made by mixing 242 g of TRIS base, 57.1 mL glacial acetic acid, 100 mL of 0.5 M EDTA in water, finally adjusting the volume to 1 L.
5. Whenever water is mentioned in the context of buffer composition, we refer to ultrapure water with resistivity 18.2 MΩcm (at 25°C) (referred to as Milli-Q water when using water purification equipment from the Millipore Corporation).
6. DNA in stock solutions at concentrations of 100–500 μg/mL is very viscous and hard to pipette accurately. Tip the tube sideways and suck in the solution very slowly to ensure that the correct amount of DNA is withdrawn. (For λ-DNA from New England Biolabs the stock solution is 500 μg/mL, so 25 μL of the solution is added to 225 μL of 0.5× TBE in a 1.5 mL microcentrifuge tube.)

   When working with lambda phage DNA, it may be advisable to heat it to 50°C for 10 min in a microcentrifuge tube heater and quench in icy water to avoid concatamers due to the hybridization of the single-strand overhangs.
7. One way of obtaining sequence information from DNA stretched in nanochannels is to tag specific sequences with a bright fluorophore. The most common way to do this is to use an enzyme that nicks the DNA at a specific sequence and subsequently repair that nick with a ligase and polymerase that incorporate fluorescent nucleotides [35, 36]. The recognition sites for commercially available nicking enzymes range

from four to seven bases in length but a recent report used a mutated CRISPR/Cas9 system to obtain a recognition site size of 23 bases [54]. In recent studies, methyltransferases have been used for the same type of experiments, where the main advantage is that the DNA is not damaged as part of the labeling process [55]. The result is a DNA stretched in nanochannels with a series of dots at specific distances that represent the underlying sequence. This principle has gained increasing attention and been commercialized via BioNanoGenomics.

8. An alternative way of obtaining sequence information is affinity-based labeling. In these assays, the principle is that the affinity of the YOYO-dye used to stain the DNA is altered in some way to make its binding sequence selective. Two main strategies have been presented in the literature. The first is to locally melt the DNA by increasing the temperature and/or adding formamide that weakens the hydrogen bonds between the bases [37]. Since AT-bases are connected via two hydrogen bonds and GC-bases by three, AT-bases melt at a lower temperature. Since YOYO-1 only binds to base-paired DNA, it will bind preferably to GC-rich regions in a partly melted DNA and an intensity variation along the DNA, where GC-regions are bright and AT-regions are dark, will be formed.

   A different way of forming the affinity-based barcode is to add netropsin as the same time as YOYO is added. Netropsin is a molecule that has a strong preference for AT-rich DNA and hence blocks those regions from YOYO binding. As a consequence, YOYO will mostly bind to GC-rich regions, and the result is again an intensity variation along the DNA where AT-rich regions are dark and GC-rich regions are bright [38]. Competitive binding-based barcodes have recently been extensively used for identification and characterization of bacterial plasmids coding for antibiotic resistance [56–60] and bacterial typing [61].

9. BME is a highly toxic chemical that serves as a biological antioxidant by scavenging oxygen and hydroxyl radicals in the buffer, thereby preventing photobleaching and photoinduced damage (photonicking) of the DNA.

   An enzymatic oxygen scavenger system may constitute a useful alternative when reducing agents cannot be used. It consists of 0.2 mg/mL glucose oxidase, 0.04 mg/mL catalase, and 4 mg/mL β-D-glucose (available from Sigma-Aldrich). The oxygen scavenger system can be combined with BME but typically does not provide any additional benefit for the experiments listed.

10. One useful option in a fluorescence microscope is a unit that sends a selected field of view through two different optical paths and projects the resulting images on two separate areas

of the CCD. This allows the user to acquire two (or more) colors or two polarization directions simultaneously. Existing systems include DV2™ from Photometrics and OptoSplit™ from Cairn Research.

11. To improve imaging resolution, a wide range of novel techniques have been developed, each one capable of reaching a resolution of below 100 nm [49]. They essentially fall in three categories: local quenching of the fluorescence emission (STED), repeated photoactivation and subsequent imaging of a subset of the fluorophores in the sample (STORM, FPALM), and structured illumination (SIM).

    Most imaging is carried out with B/W cameras giving information on the intensity in each pixel. For additional contrast information, multicolor (spectroscopic) or fluorescence life-time imaging (FLIM) may be utilized.

12. For affinity-based optical DNA mapping, described in **Note 8**, the theoretical framework for creating theoretical barcodes, comparing experimental and theoretical barcodes, forming consensus barcodes from several individual barcodes etc. can be found in the literature [56, 62–64].

13. In order to expose the DNA to a gradual change in confinement in one single chip, it is possible to use funnel-like channels [12, 65]. This is an analogue to force spectroscopy techniques using optical tweezers that allows for probing of low DNA extensions, corresponding to forces in the femtonewton regime, without anchoring the molecules. Another feature that can be added to the chip is demonstrated in Fig. 4 (right). In this chip design, a nanoslit is etched orthogonal to the nanochannels. This allows for enrichment of DNA in the nanogrooves by applying moderate positive pressures at both ends of the nanochannels. If the slit is sufficiently shallow, entropy keeps the DNA in the grooves while buffer flows through the slit. This design also allows for changing the chemical environment of the DNA, by flushing the desired solution in the slit, while monitoring the DNA in real time [32, 66].

14. When analyzing long, genomic DNA, extra care must be taken due to the relatively large size of the molecules. For intermediate size DNA such as from bacteria, a meandering nanochannel can be used [67], so that the entire DNA can be visualized in one singe frame. Considering human DNA, it can be noted that the largest single DNA molecule has a fully extended length of over 8 cm (chromosome 1). If the DNA molecule is too long for the whole molecule to be easily extended in a single nanochannel, one possibility is to stretch it by shear flow [68, 69] in a device made by conventional photolithography.

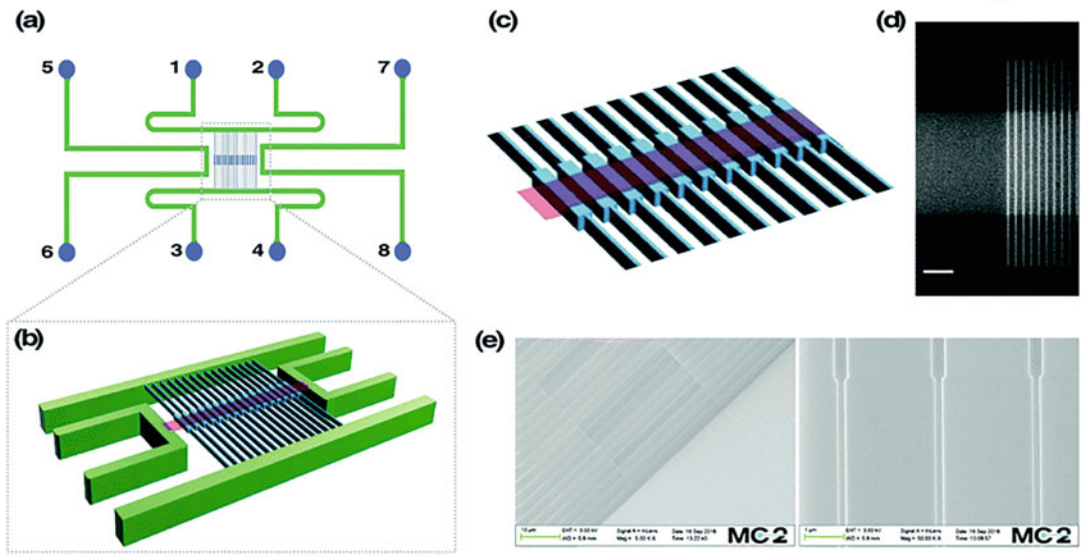

Fig. 4 (**a**) Schematic representation of the nanofluidic chip, where 1–4 are loading holes connected to microchannels, which in turn are connected to the nanochannels. 5–8 are loading holes connected to microchannels, which are then connected by a nanoslit at the center. (**b**) Zoomed-in image showing the center region where the nanochannels intercept with the nanoslit. (**c**) Zoomed-in view of the reaction chamber formed by the nanochannel-nanoslit. (**d**) Fluorescence microscope image showing the reaction chamber filled with fluorescein. (**e**) SEM images showing the nanoslit aligned to the nanochannels forming the reaction chamber. (Reproduced from Ref. [32] with permission from The Royal Society of Chemistry)

With this approach, there is no need for nanofabrication. However, it is a dynamic system in which the DNA conformation will not be at equilibrium as compared to DNA confined in nanochannels.

15. Complex micro-nanofluidic design involving multiple sets of micro and nanochannels in a single device and simple automation with the help of a pressure pump and image acquisition tools enables multiplexing. A recent development is the use of a parallelized nanofluidic device with ten sets of nanochannels, automated using a simple routine to enable analysis of ten samples simultaneously. Such a device increases the throughput and also minimizes laborious data collection process [70].
16. Even without an e-beam writer, slit-like channels (depth in the nanometer range and widths larger than 0.5 μm) can readily be defined with UV lithography and carefully tuned RIE etching [71–73]. Fabrication of slit-like channels can be done with other methods like injection molding, nanoimprint lithography, etc. and using polymeric materials like PDMS, PMMA, or COC [74].
17. Alignment marks can alternatively be formed by anisotropic RIE etching and in the case of silicon also through anisotropic

wet etching using, for example, KOH. If etching is used to define the alignment marks, it is important that they provide a sufficient contrast for the alignment in the mask aligner. An etch depth of at least 200 nm is recommended. For metal alignment marks, it is also possible to first deposit a layer of metal and subsequently spin on and pattern a photoresist and in a last step etch away the exposed metal. Al is commonly etched using either a wet etch using phosphoric acid or a dry etch containing chlorine chemistry. Au is commonly etched by using wet etches of either potassium iodine or aqua regia (1:3 HNO_3:HCl).

18. Instead of using chemicals, the resist can be stripped by an oxygen plasma treatment. However, this is not recommended since it can burn the resist, making it very hard to remove, and also induces roughness on the sample surface.
19. Examples include micromilling, deep reactive ion etching (DRIE) or ultrasonic drilling. However, these techniques often demand some specialized equipment, which is very expensive compared to that needed for powder blasting.
20. Instead of using a soft film in order to mask the wafers/chips during powder blasting, a metal mask defined in a thick brass plate can be used. The chip is then attached to the metal mask using reversible thermal glue. It should be noted that since the metal mask is hard, it will also be degraded by the powder blasting, which attacks hard surfaces.
21. Polymer-based devices are generally sealed using polymer fusion bonding. The device is bonded to a lid with a polymer film by heating until the polymer layers on the chip and lid intermix. The combination of polymer compositions and temperatures must be carefully chosen to create a sufficiently strong bond while maintaining the structural integrity of the micro- and nanochannels. Polysilsesquioxane (PSQ), for example, is a Si-based inorganic–organic polymer with very good mechanical properties that has been demonstrated to work well in bonding micro- and nanochannels [71, 75]. Anodic bonding is the standard technique to bond borosilicate glass to silicon, also for silicon with a hydrophilic oxide layer, but it might cause wide nanochannels (nanoslits) to collapse.
22. The Piranha-based protocol can be used to bond silicon with a thin layer of oxide (<150 nm) and borosilicate glass. However, the final annealing should in this case be done at 400–450°C to avoid excessive strain due to the difference in thermal expansion coefficient between silicon and glass [73].
23. BME degrades in the presence of oxygen, and therefore, a small amount should be transferred to a microcentrifuge tube and used for the experiments in order to avoid opening the main

bottle too many times. The main bottle should be filled with nitrogen after each time it is opened. A sealed bottle should be stable for at least 3 years. The BME in a mixed loading buffer will last approximately one day.

24. For chips that are difficult to wet, for example in the case of hydrophobic materials or dead-end channels, critical point wetting [76] can be used. However, critical point wetting requires that the material used is capable of withstanding at least the temperature at the critical point of water, $T = 374°C$.
25. Using lipid bilayers is an efficient way of passivating nanofluidic structures [77]. Lipid bilayers are superior to common passivating strategies in microfluidics, such as nonspecific binding of BSA, since a lipid bilayer is a 2D liquid and hence very smooth and defect free due to its inherent self-repair capability. Lipid bilayers have been used in several studies of DNA-protein interactions in nanochannels [78, 79].
26. The frame rate should be selected based on the timescales of interest. Long exposure times might blur the image due to drift and diffusion of the DNA. Signal-to-noise might become insufficient for very short exposure times. For typical imaging applications, 10 fps is a suitable choice. Very short exposure times enable detailed studies of dynamics and fluctuations, typically occurring at higher rates than 10 Hz. Long exposure times can on the other hand be used to discern bound molecules from freely diffusing molecules. It has also been shown that altering the exposure times makes it possible to obtain binding kinetics for transcription factors on DNA [80].
27. It should be noted that to be mathematically rigorous an Airy function should be used for an ideal optical system rather than the more convenient-to-use Gaussian approximation. Furthermore, to fully optimize the analysis, it has been shown that a careful choice of fitting function that closely mimics the real PSF will give a slight but significant improvement.

Acknowledgments

This work was supported by the European Community's Horizon2020 (BeyondSeq 634890) (JOT, JPB and FW), the European Research Council (Consolidator Grant nanoDNArepair, 866238) (FW), the Swedish Research Council (2020-03400) (FW), ERA-NET EuroNanoMed II (NanoDiaBac, E0748601) (JOT, JPB and FW). JOT and JPB acknowledge support from NanoLund at Lund University. SKK, JF and FW acknowledge support from MyFab Chalmers.

References

1. Tegenfeldt JO, Prinz C, Cao H, Chou S, Reisner WW, Riehn R et al (2004) The dynamics of genomic-length DNA molecules in 100-nm channels. Proc Natl Acad Sci U S A 101(30): 10979–10983
2. Frykholm K, Müller V, Sriram KK, Dorfman KD, Westerlund F (2022) DNA in nanochannels – theory and applications. Q Rev Biophys 55:1–83. https://doi.org/10.1017/S0033583522000117
3. Vologodskii A, Cozzarelli N (1995) Modeling of long-range electrostatic interactions in DNA. Biopolymers 35(3):289–296
4. Daoud M, de Gennes PG (1977) Statistics of macromolecular solutions trapped in small pores. J Phys 38:85–93
5. Turban L (1984) Conformation of confined macromolecular chains - crossover between slit and capillary. J Phys 45(2):347–353
6. Odijk T (1983) On the statistics and dynamics of confined or entangled stiff polymers. Macromolecules 16(8):1340–1344
7. Frykholm K, Alizadehheidari M, Fritzsche J, Wigenius J, Modesti M, Persson F et al (2014) Probing physical properties of a DNA-protein complex using nanofluidic channels. Small 10(5):884–887. https://doi.org/10.1002/smll.201302028
8. Yang YZ, Burkhardt TW, Gompper G (2007) Free energy and extension of a semiflexible polymer in cylindrical confining geometries. Phys Rev E 76(1):011804. https://doi.org/10.1103/PhysRevE.76.011804
9. Smithe TSC, Iarko V, Muralidhar A, Werner E, Dorfman KD, Mehlig B (2015) Finite-size corrections for confined polymers in the extended de Gennes regime. Phys Rev E 92(6):5. https://doi.org/10.1103/PhysRevE.92.062601
10. Werner E, Mehlig B (2015) Scaling regimes of a semiflexible polymer in a rectangular channel. Phys Rev E 91(5):5. https://doi.org/10.1103/PhysRevE.91.050601
11. Reisner W, Pedersen JN, Austin RH (2012) DNA confinement in nanochannels: physics and biological applications. Rep Prog Phys 75(10):106601. https://doi.org/10.1088/0034-4885/75/10/106601
12. Persson F, Utko P, Reisner W, Larsen NB, Kristensen A (2009) Confinement spectroscopy: probing single DNA molecules with tapered nanochannels. Nano Lett 9(4): 1382–1385. https://doi.org/10.1021/nl803030e
13. Persson F, Tegenfeldt JO (2010) DNA in nanochannels - directly visualizing genomic information. Chem Soc Rev 39(3):985–999. https://doi.org/10.1039/B912918A
14. de Gennes PG (1979) Scaling concepts in polymer physics. Cornell University Press, Ithaca
15. Doi M, Edwards SF (1986) The theory of polymer dynamics, The international series of monographs on physics. Oxford University Press, Inc., New York
16. Rubinstein M, Colby RH (2003) Polymer physics. Oxford University Press, New York
17. Reisner W, Morton KJ, Riehn R, Wang YM, Yu ZN, Rosen M et al (2005) Statics and dynamics of single DNA molecules confined in nanochannels. Phys Rev Lett 94(19):196101
18. Persson F, Westerlund F, Tegenfeldt JO, Kristensen A (2009) Local conformation of confined DNA studied using emission polarization anisotropy. Small 5(2):190–193
19. Iarko V, Werner E, Nyberg LK, Müller V, Fritzsche J, Ambjörnsson T et al (2015) Extension of nanoconfined DNA: quantitative comparison between experiment and theory. Phys Rev E 92(6):062701
20. Werner E, Mehlig B (2014) Confined polymers in the extended de Gennes regime. Phys Rev E 90(6):5. https://doi.org/10.1103/PhysRevE.90.062602
21. Gupta D, Miller JJ, Muralidhar A, Mahshid S, Reisner W, Dorfman KD (2015) Experimental evidence of weak excluded volume effects for nanochannel confined DNA. ACS Macro Lett 4(7):759–763. https://doi.org/10.1021/acsmacrolett.5b00340
22. Ma Z, Dorfman KD (2020) Diffusion of knots along DNA confined in nanochannels. Macromolecules 53(15):6461–6468. https://doi.org/10.1021/acs.macromol.0c00561
23. Gupta D, Bhandari AB, Dorfman KD (2018) Evaluation of blob theory for the diffusion of DNA in nanochannels. Macromolecules 51(5): 1748–1755. https://doi.org/10.1021/acs.macromol.7b02270
24. Krog J, Alizadehheidari M, Werner E, Bikkarolla SK, Tegenfeldt JO, Mehlig B et al (2018) Stochastic unfolding of nanoconfined DNA: experiments, model and Bayesian analysis. J Chem Phys 149(21):215101. https://doi.org/10.1063/1.5051319
25. Riehn R, Lu MC, Wang YM, Lim SF, Cox EC, Austin RH (2005) Restriction mapping in nanofluidic devices. Proc Natl Acad Sci U S A 102(29):10012–10016

26. Wang YM, Tegenfeldt JO, Reisner W, Riehn R, Guan XJ, Guo L et al (2005) Single-molecule studies of repressor-DNA interactions show long-range interactions. Proc Natl Acad Sci U S A 102(28):9796–9801
27. Öz R, Howard SM, Sharma R, Törnkvist H, Ceppi I, Kk S et al (2020) Phosphorylated CtIP bridges DNA to promote annealing of broken ends. Proc Natl Acad Sci 117(35): 21403–21412. https://doi.org/10.1073/pnas.2008645117
28. Jiang K, Rocha S, Westling A, Kesarimangalam S, Dorfman KD, Wittung-Stafshede P et al (2018) Alpha-Synuclein modulates the physical properties of DNA. Chem Eur J 24(58):15685–15690. https://doi.org/10.1002/chem.201803933
29. Jiang K, Zhang C, Guttula D, Liu F, Jeroen A, Lavelle C et al (2015) Effects of Hfq on the conformation and compaction of DNA. Nucleic Acids Res 43(8):4332–4341. https://doi.org/10.1093/nar/gkv268
30. Jiang K, Humbert N, S KK, Rouzina I, Mely Y, Westerlund F (2021) The HIV-1 nucleocapsid chaperone protein forms locally compacted globules on long double-stranded DNA. Nucleic Acids Res 49(8):4550–4563. https://doi.org/10.1093/nar/gkab236
31. Zhang C, Guttula D, Liu F, Malar PP, Ng SY, Dai L et al (2013) Effect of H-NS on the elongation and compaction of single DNA molecules in a nanospace. Soft Matter 9(40): 9593–9601. https://doi.org/10.1039/c3sm51214b
32. Öz R, Kk S, Westerlund F (2019) A nanofluidic device for real-time visualization of DNA–protein interactions on the single DNA molecule level. Nanoscale 11(4):2071–2078. https://doi.org/10.1039/c8nr09023h
33. Öz R, Wang JL, Guerois R, Goyal G, Kk S, Ropars V et al (2021) Dynamics of Ku and bacterial non-homologous end-joining characterized using single DNA molecule analysis. Nucleic Acids Res 49(5):2629–2641. https://doi.org/10.1093/nar/gkab083
34. Jeffet J, Margalit S, Michaeli Y, Ebenstein Y (2021) Single-molecule optical genome mapping in nanochannels: multidisciplinarity at the nanoscale. Essays Biochem 65(1): 51–66. https://doi.org/10.1042/ebc20200021
35. Jo K, Dhingra DM, Odijk T, de Pablo JJ, Graham MD, Runnheim R et al (2007) A single-molecule barcoding system using nanoslits for DNA analysis. Proc Natl Acad Sci U S A 104(8):2673–2678
36. Das SK, Austin MD, Akana MC, Deshpande P, Cao H, Xiao M (2010) Single molecule linear analysis of DNA in nano-channel labeled with sequence specific fluorescent probes. Nucleic Acids Res 38(18):e177. https://doi.org/10.1093/nar/gkq673
37. Reisner W, Larsen NB, Silahtaroglu A, Kristensen A, Tommerup N, Tegenfeldt JO et al (2010) Single-molecule denaturation mapping of DNA in nanofluidic channels. Proc Natl Acad Sci 107(30):13294–13299
38. Nyberg LK, Persson F, Berg J, Bergstrom J, Fransson E, Olsson L et al (2012) A single-step competitive binding assay for mapping of single DNA molecules. Biochem Biophys Res Commun 417(1):404–408. https://doi.org/10.1016/j.bbrc.2011.11.128
39. Frykholm K, Nyberg LK, Lagerstedt E, Noble C, Fritzsche J, Karami N et al (2015) Fast size-determination of intact bacterial plasmids using nanofluidic channels. Lab Chip 15(13):2739–2743. https://doi.org/10.1039/c5lc00378d
40. Basak R, Liu F, Qureshi S, Gupta N, Zhang C, De Vries R et al (2019) Linearization and labeling of single-stranded DNA for optical sequence analysis. J Phys Chem Lett 10(3): 316–321. https://doi.org/10.1021/acs.jpclett.8b03465
41. Madou MJ (2011) Fundamentals of microfabrication and nanotechnology, 3rd edn. CRC Press, Boca Raton
42. Reisner W, Beech JP, Larsen NB, Flyvbjerg H, Kristensen A, Tegenfeldt JO (2007) Nanoconfinement-enhanced conformational response of single DNA molecules to changes in ionic environment. Phys Rev Lett 99(5): 058302. https://doi.org/10.1103/PhysRevLett.99.058302
43. Nyberg L, Persson F, Åkerman B, Westerlund F (2013) Heterogeneous staining: a tool for studies of how fluorescent dyes affect the physical properties of DNA. Nucleic Acids Res 41: e184. https://doi.org/10.1093/nar/gkt755
44. Mertz J (2010) Introduction to optical microscopy. Roberts and Company Publishers, Greenwood Village
45. Glazer AN, Rye HS (1992) Stable dye-DNA intercalation complexes as reagents for high-sensitivity fluorescence detection. Nature 359(6398):859–861
46. Spielmann HP, Wemmer DE, Jacobsen JP (1995) Solution structure of a DNA complex with the fluorescent bis-intercalator TOTO determined by NMR-spectroscopy. Biochemistry 34(27):8542–8553

47. Kundukad B, Yan J, Doyle PS (2014) Effect of YOYO-1 on the mechanical properties of DNA. Soft Matter 10(48):9721–9728. https://doi.org/10.1039/c4sm02025a
48. Lerman LS (1961) Structural considerations in interaction of DNA and acridines. J Mol Biol 3(1):18–30
49. Reinert KE (1973) DNA stiffening and elongation caused by binding of ethidium bromide. Biochim Biophys Acta 319(2):135–139
50. Thamdrup LH, Persson F, Bruus H, Kristensen A, Flyvbjerg H (2007) Experimental investigation of bubble formation during capillary filling of SiO2 nanoslits. Appl Phys Lett 91(16):163505. https://doi.org/10.1063/1.2801397
51. Levy SL, Mannion JT, Cheng J, Reccius CH, Craighead HG (2008) Entropic unfolding of DNA molecules in nanofluidic channels. Nano Lett 8(11):3839–3844. https://doi.org/10.1021/nl802256s
52. Persson F (2009) Nanofluidics for single molecule DTU nanotech - department of micro- and nanotechnology. Technical University of Denmark, Kongens Lyngby
53. Thompson RE, Larson DR, Webb WW (2002) Precise nanometer localization analysis for individual fluorescent probes. Biophys J 82(5): 2775–2783
54. McCaffrey J, Sibert J, Zhang B, Zhang YG, Hu WH, Riethman H et al (2016) CRISPR-CAS9 D10A nickase target-specific fluorescent labeling of double strand DNA for whole genome mapping and structural variation analysis. Nucleic Acids Res 44(2):8. https://doi.org/10.1093/nar/gkv878
55. Grunwald A, Dahan M, Giesbertz A, Nilsson A, Nyberg LK, Weinhold E et al (2015) Bacteriophage strain typing by rapid single molecule analysis. Nucleic Acids Res 43 (18):e117-e. https://doi.org/10.1093/nar/gkv563
56. Nilsson AN, Emilsson G, Nyberg LK, Noble C, Stadler LS, Fritzsche J et al (2014) Competitive binding-based optical DNA mapping for fast identification of bacteria - multi-ligand transfer matrix theory and experimental applications on Escherichia coli. Nucleic Acids Res 42(15):e118. https://doi.org/10.1093/nar/gku556
57. Muller V, Karami N, Nyberg LK, Pichler C, Pedreschi PCT, Quaderi S et al (2016) Rapid tracing of resistance plasmids in a nosocomial outbreak using optical DNA mapping. ACS Infect Dis. 2(5):322–328. https://doi.org/10.1021/acsinfecdis.6b00017
58. Bikkarolla SK, Nordberg V, Rajer F, Müller V, Kabir MH, KK S et al (2019) Optical DNA mapping combined with Cas9-targeted resistance gene identification for rapid tracking of resistance plasmids in a neonatal intensive care unit outbreak. MBio 10(4):e00347–e00319. https://doi.org/10.1128/mBio.00347-19
59. Kk S, Ekedahl E, Hoang NTB, Sewunet T, Berglund B, Lundberg L et al (2022) High diversity of blaNDM-1-encoding plasmids in Klebsiella pneumoniae isolated from neonates in a Vietnamese hospital. Int J Antimicrob Agents 59(2):106496. https://doi.org/10.1016/j.ijantimicag.2021.106496
60. Lin Y-L, Sewunet T, Kk S, Giske CG, Westerlund F (2020) Optical maps of plasmids as a proxy for clonal spread of MDR bacteria: a case study of an outbreak in a rural Ethiopian hospital. J Antimicrob Chemother 75(10): 2804–2811. https://doi.org/10.1093/jac/dkaa258
61. Müller V, Nyblom M, Johnning A, Wrande M, Dvirnas A, Kk S et al (2020) Cultivation-free typing of bacteria using optical DNA mapping. ACS Infect Dis 6(5):1076–1084. https://doi.org/10.1021/acsinfecdis.9b00464
62. Dvirnas A, Pichler C, Stewart CL, Quaderi S, Nyberg LK, Müller V et al (2018) Facilitated sequence assembly using densely labeled optical DNA barcodes: a combinatorial auction approach. PLoS One 13(3):e0193900. https://doi.org/10.1371/journal.pone.0193900
63. Dvirnas A, Stewart C, Müller V, Bikkarolla SK, Frykholm K, Sandegren L et al (2021) Detection of structural variations in densely-labelled optical DNA barcodes: a hidden Markov model approach. PLoS One 16(11):e0259670. https://doi.org/10.1371/journal.pone.0259670
64. Torstensson E, Goyal G, Johnning A, Westerlund F, Ambjörnsson T (2021) Combining dense and sparse labeling in optical DNA mapping. PLoS One 16(11):e0260489. https://doi.org/10.1371/journal.pone.0260489
65. Frykholm K, Berntsson RP-A, Claesson M, Laura OR, Stenmark P et al (2016) DNA compaction by the bacteriophage protein Cox studied on the single DNA molecule level using nanofluidic channels. Nucleic Acids Res 44: gkw352. https://doi.org/10.1093/nar/gkw352
66. Sharma R, Kk S, Holmstrom ED, Westerlund F (2020) Real-time compaction of nanoconfined DNA by an intrinsically disordered macromolecular counterion. Biochem Biophys Res

Commun 533(1):175–180. https://doi.org/10.1016/j.bbrc.2020.06.051

67. Freitag C, Noble C, Fritzsche J, Persson F, Reiter-Schad M, Nilsson AN et al (2015) Visualizing the entire DNA from a chromosome in a single frame. Biomicrofluidics 9(4): 044114. https://doi.org/10.1063/1.4923262
68. Perkins TT, Smith DE, Chu S (1997) Single polymer dynamics in an elongational flow. Science 276(5321):2016–2021
69. Marie R, Pedersen JN, Bauer DLV, Rasmussen KH, Yusuf M, Volpi E et al (2013) Integrated view of genome structure and sequence of a single DNA molecule in a nanofluidic device. Proc Natl Acad Sci 100(13):4893–4898. https://doi.org/10.1073/pnas.1214570110
70. Kk S, Lin Y-L, Sewunet T, Wrande M, Sandegren L, Giske C et al (2021) A parallelized nanofluidic device for high-throughput optical DNA mapping of bacterial plasmids. Micromachines 12(10):1234. https://doi.org/10.3390/mi12101234
71. Sriram KK, Yeh J-W, Lin Y-L, Chang Y-R, Chou C-F (2014) Direct optical mapping of transcription factor binding sites on field-stretched λ-DNA in nanofluidic devices. Nucleic Acids Res 42(10):e85-e. https://doi.org/10.1093/nar/gku254
72. Yeh J-W, Taloni A, Chen Y-L, Chou C-F (2012) Entropy-driven single molecule tug-of-war of DNA at micro–nanofluidic interfaces. Nano Lett 12(3):1597–1602. https://doi.org/10.1021/nl2045292
73. Persson F, Thamdrup LH, Mikkelsen MBL, Jaarlgard SE, Skafte-Pedersen P, Bruus H et al (2007) Double thermal oxidation scheme for the fabrication of SiO2 nanochannels. Nanotechnology 18(24):245301. https://doi.org/10.1088/0957-4484/18/24/245301
74. Chantiwas R, Park S, Soper SA, Kim BC, Takayama S, Sunkara V et al (2011) Flexible fabrication and applications of polymer nanochannels and nanoslits. Chem Soc Rev 40(7): 3677. https://doi.org/10.1039/c0cs00138d
75. Gu J, Gupta R, Chou C-F, Wei Q, Zenhausern F (2007) A simple polysilsesquioxane sealing of nanofluidic channels below 10 nm at room temperature. Lab Chip 7(9):1198. https://doi.org/10.1039/b704851c
76. Riehn R, Austin RH (2006) Wetting micro- and nanofluidic devices using supercritical water. Anal Chem 78(16):5933–5934
77. Persson F, Fritzsche J, Mir KU, Modesti M, Westerlund F, Tegenfeldt JO (2012) Lipid-based passivation in nanofluidics. Nano Lett 12:2260–2265. https://doi.org/10.1021/nl204535h
78. Fornander LH, Frykholm K, Fritzsche J, Araya J, Nevin P, Werner E et al (2016) Visualizing the nonhomogeneous structure of RAD51 filaments using nanofluidic channels. Langmuir 32(33):8403–8412. https://doi.org/10.1021/acs.langmuir.6b01877
79. Frykholm K, Berntsson RPA, Claesson M, de Battice L, Odegrip R, Stenmark P et al (2016) DNA compaction by the bacteriophage protein Cox studied on the single DNA molecule level using nanofluidic channels. Nucleic Acids Res 44(15):7219–7227. https://doi.org/10.1093/nar/gkw352
80. Elf J, Li GW, Xie XS (2007) Probing transcription factor dynamics at the single-molecule level in a living cell. Science 316(5828): 1191–1194